



# Assessing event magnitude and target water depth for marine-target impacts: Ocean resurge deposits in the Chicxulub M0077A drill core compared

J. Ormö <sup>a,\*</sup>, S.P.S. Gulick <sup>b,c</sup>, M.T. Whalen <sup>d</sup>, D.T. King Jr. <sup>e</sup>, E. Sturkell <sup>f</sup>, J. Morgan <sup>g</sup>

<sup>a</sup> Centro de Astrobiología (INTA-CSIC), Ctra Torrejon a Ajalvir km4, 28850 Torrejon de Ardoz, Spain

<sup>b</sup> Inst. for Geophysics & Dept. of Geological Sciences, 10100 Burnet Rd Bldg. ROC, Jackson School of Geosciences, Univ. of Texas at Austin, Austin, TX 78758, USA

<sup>c</sup> Center for Planetary Systems Habitability, Univ. of Texas at Austin, Austin, TX 78712, USA

<sup>d</sup> Dept. of Geosciences, University of Alaska Fairbanks, USA

<sup>e</sup> Dept. of Geosciences, 2058 Memorial Coliseum, Auburn University, Auburn, AL 36849, USA

<sup>f</sup> Earth Sciences Centre, Univ. of Gothenburg, Sweden

<sup>g</sup> Dept. of Earth Science and Engineering, Imperial College London, UK



## ARTICLE INFO

### Article history:

Received 22 December 2019

Received in revised form 24 March 2021

Accepted 27 March 2021

Available online xxxx

Editor: W.B. McKinnon

### Keywords:

marine-target crater

resurge deposits

Chicxulub crater

Site M0077

suevite

melt water interaction

## ABSTRACT

The rim wall of water formed from even a modestly-sized marine impact may be kilometers in height. Although modeling has shown that this wave swiftly breaks and relatively rapidly loses energy during outwards travel from the impact site, the portion of the rim wall that collapses inwards may generate a resurge flow with tremendous transport energy. Here we compare the deposits generated by this ocean resurge inside one of the largest marine-target craters on Earth, the 200-km wide Chicxulub crater, Yucatán Peninsula, México, with resurge deposits (breccias) in eight drill cores from five other marine-target craters in Sweden and the United States. Examination of the wide range of cored locations within the craters, and target water depths ( $H$ ) relative to modeled projectile diameters ( $d$ ) reveal a high correlation between location, average clast frequency ( $(N)$ ), and  $d/H$  from which any of the four variables can be obtained. The relationship shown here may provide an important tool for diagnosing marine impact cratering processes where there is limited understanding of crater size and/or paleobathymetry.

© 2021 The Authors. Published by Elsevier B.V. This is an open access article under the CC BY-NC-ND license (<http://creativecommons.org/licenses/by-nc-nd/4.0/>).

## 1. Introduction

A marine target environment influences both the excavation and modification stages of impact cratering depending on relative target water depth (e.g., Gault and Sonett, 1982), especially with regard to water resurge (Ormö et al., 2007, 2010a). If the ratio between projectile diameter ( $d$ ) and target water depth ( $H$ ) is  $>0.1$  a lower part of the crater develops also in the seafloor (e.g., Gault and Sonett, 1982; Wünnemann et al., 2007). The upper rim of the water cavity collapses outward forming an outward-moving 'rim wave tsunami' (Wünnemann et al., 2007) whereas the lower parts collapse inward as a 'resurge' (Ormö et al., 2007). The 200-km diameter Chicxulub impact crater formed 66.0 Ma on a continental margin in a marine setting by the impact of a  $\sim$ 12.2-km wide asteroid (Gulick et al., 2008; Artemieva et al., 2017). Based on the

earlier International Continental scientific Drilling Program (ICDP) Site Yaxcopoil-1 at Chicxulub (Fig. 1), Goto et al. (2004) presented evidence for resurge of water into the newly formed crater.

The time for a resurge to enter and fill a crater, flow velocities, and transport capacities have been analyzed by numerical simulation methods. For the 7.5-km wide Lockne crater, Sweden, Ormö and Miyamoto (2002) calculated a 30 min resurge for a target water depth of 200 m and up to 4x faster for 500 m depth. Similar duration was later estimated for a 500-m target water depth by more advanced 3-D modeling that predicted resurge could transport up to meter-sized particles whereas objects larger than 10 m would remain where they sank to the seafloor (Lindström et al., 2005a). Gulick et al. (2019) estimate that resurge at the newly formed Chicxulub crater would submerge the peak ring within  $\sim$ 30–60 min post-impact, but that complete flooding of the crater likely took hours.

Sedimentological analysis and comparisons with data, experiments, and simulations from other marine-target craters allow reconstruction of the events behind Chicxulub's graded suevite (Fig. 2). In a marine impact, if the relative water depth is large

\* Corresponding author.

E-mail addresses: [ormoj@cab.inta-csic.es](mailto:ormoj@cab.inta-csic.es) (J. Ormö), [sean@ig.utexas.edu](mailto:sean@ig.utexas.edu) (S.P.S. Gulick), [mtwhalen@alaska.edu](mailto:mtwhalen@alaska.edu) (M.T. Whalen), [kingdat@auburn.edu](mailto:kingdat@auburn.edu) (D.T. King), [erik.sturkell@gvc.gu.se](mailto:erik.sturkell@gvc.gu.se) (E. Sturkell), [j.morgan@imperial.ac.uk](mailto:j.morgan@imperial.ac.uk) (J. Morgan).

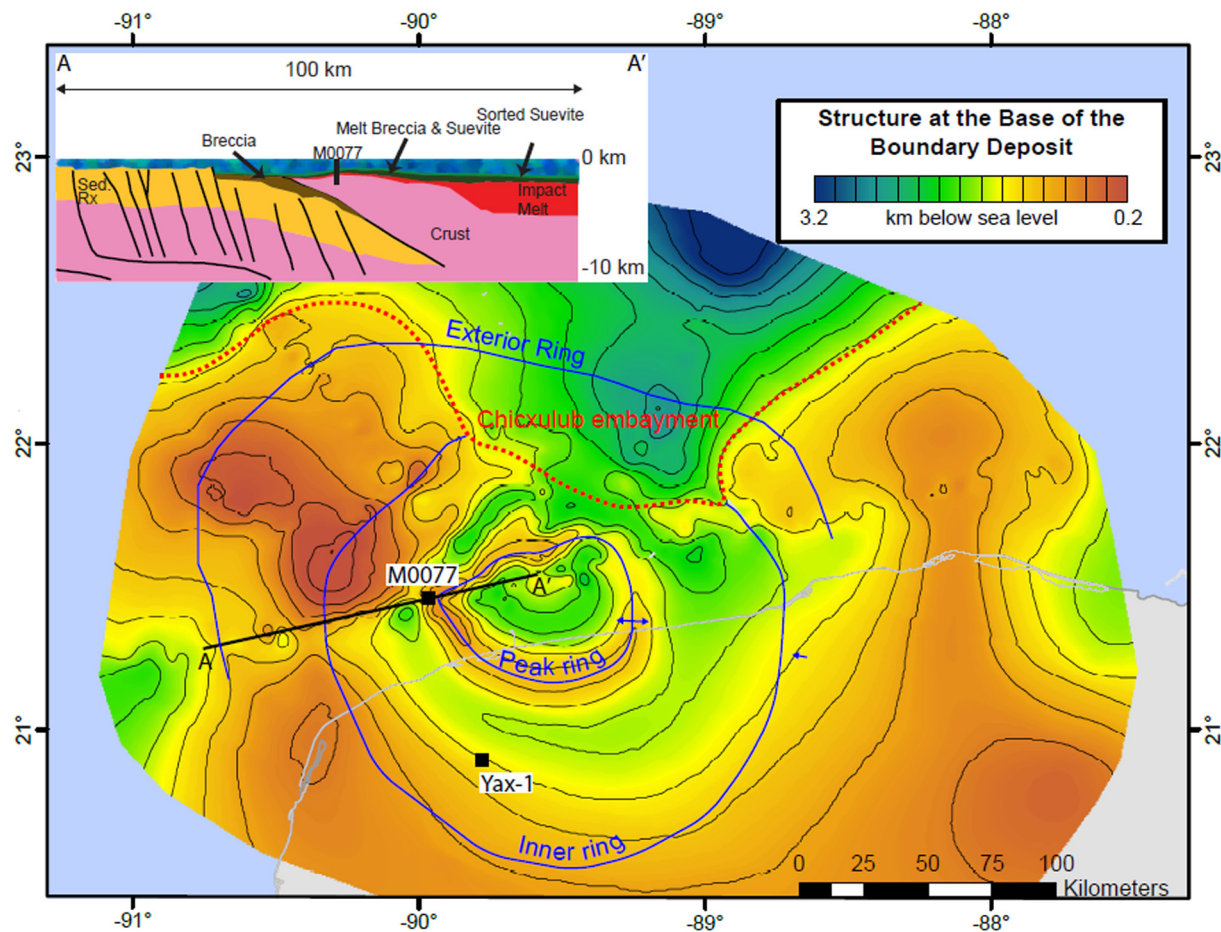


**Fig. 1.** The Chicxulub impact crater ring structures as reviewed in Gulick et al. (2013) based on geophysical data overlying a structure contour map of top of the K-Pg boundary deposit modified from Sanford et al. (2016). Inner ring onshore is traced inside the ring of cenotes that are present within the ring faults. Inset cross-section based on a seismic profile is shown from A-A' where the geologic interpretation is from Gulick et al. (2019) wherein breccia (brown) associated with inward transport are distinguished from melt breccia and suevite (dark green) associated with resurge and melt-water interactions, and sorted suevite (light green) deposited in a flooded crater. Drillsites ICDP Yaxcopoil-1 (Yax-1) within the terrace zone and IODP-ICDP Site M0077 on top of the peak ring are shown. (For interpretation of the colors in the figure(s), the reader is referred to the web version of this article.)

enough to let the resurge pass the rim from all sides (such as at the Lockne crater, Sweden) the resurge will cause the rise of a 'central water plume' (Ormö et al., 2007, 2010a; Wünnemann et al., 2007), which when collapsing generates an outward-moving 'anti-resurge' (Ormö et al., 2007). The collapse of the central water plume at impacts where  $d/H < 0.6$  may allow the anti-resurge to pass beyond the crater rim and a second wave, a 'collapse wave tsunami', will propagate out from the impact site (Wünnemann et al., 2007). However, if the water is much deeper on one side of the crater, as is the case for the Chicxulub crater (Gulick et al., 2008), experiments show that the deep water resurge will traverse the crater faster and may halt (i.e., create a central water plume), or even push back, the resurge at the rim on the shallow water side (Ormö et al., 2010a). A similar effect is seen also in an experiment of an oblique impact, but in this instance the resurge from the uprange side occupies the crater interior before the down-range resurge flow because of its initial proximity to the crater rim (Ormö et al., 2010a). At Chicxulub, both effects may have been combined as the water was deeper (2 km on the NE side vs  $\sim 100$  m to the SW) (Gulick et al., 2008), and the impact angle has been modeled to have been  $\sim 45\text{--}60^\circ$  above horizontal with a down-range direction to the SW (Collins et al., 2020).

One objective of the International Ocean Discovery Program (IODP)-ICDP Expedition 364 Site M0077 located on the Chicxulub peak ring (Fig. 1) was the improved understanding of marine cratering and modification processes during formation of a multi-

or peak-ring crater (Gulick et al., 2017a, 2019). At Site M0077 ( $21.45^\circ\text{N}$ ,  $89.95^\circ\text{W}$ ), core between 505.70 and 1334.73 mbsf (meters below sea floor) was recovered from the peak ring, WNW of crater center (Morgan et al., 2016) (Fig. 1). The core preserves, from top down, a sequence that begins with  $\sim 110$  m of post-impact hemipelagic and pelagic Paleogene sedimentary rocks (Unit 1) the lowermost portion of which is a 75 cm thick, transitional unit that included higher energy post-impact sedimentation (Unit 1G, cf. Whalen et al., 2020). This unit is underlain by  $\sim 130$  m (617 to 747 mbsf) of, mainly, a graded suevite (polymict impact melt-bearing breccia, Units 2A, B) although in the parts below 712.84 mbsf sections a clast-rich melt rock appears, leading to the term melt rock breccia also being used (Unit 2C, cf. Gulick et al., 2017a, 2019) (Fig. 1, Fig. 2). This sequence, in turn, overlies impact melt rock (Unit 3) and felsic basement rocks (Unit 4) (747 to 1334.73 mbsf) (Gulick et al., 2017a).

Here we estimate the effect of the marine environment on deposition of the lower, coarser parts of the graded suevite on the peak ring that at the onset of the resurge formed a  $\sim 500$ -m topographic high (Fig. 1, Fig. 2). The objective is to estimate the magnitude and timing of the resurge at this location, as well as the provenance of the material carried by the flow within the crater. Choice of this section of the graded suevite allows the use of the drill core line-logging method previously applied in studies of water-laid sediments of similar grain size fractions at several

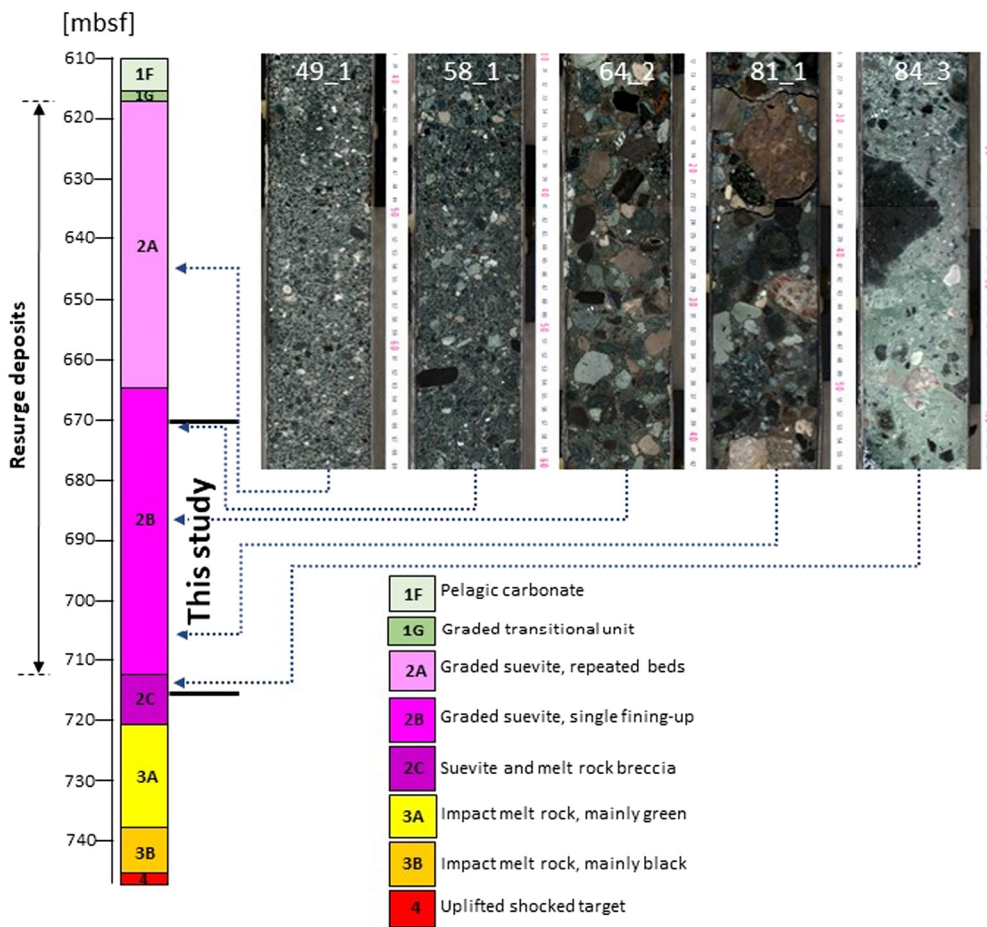


**Fig. 2.** Lithologic summary and selected core photos of relevant parts of the core used in the present study from Hole M0077A. The photo of section 49\_1 illustrates the finer grained deposits above the logged interval (i.e., above the 5 mm cut-off), and the photo of section 84\_3 shows that at the lower end of the logged interval the lithology is now in parts a clast-rich melt rock or a melt rock breccia and not a completely clastic deposit (Core log based on Gulick et al., 2017a, 2019).

other marine impact craters formed at a range of relative water depths (e.g., Ormö et al., 2007, 2009).

## 2. Methods

Line-logging of drill cores allows analysis of relative changes recorded in marine impact structure infill, including slump and resurge deposits, and has been applied on cores from Lockne, Tvären, and Vakkejokk craters in Sweden, and Chesapeake Bay Impact Structure (hereafter CBIS), Wetumpka, and Flynn Creek craters in the United States (Örmo et al., 2007, 2009, 2010b, 2019; De Marchi et al., 2019). Every clast with a length axis equal to or larger than the analytic cut-off size and that touches a line drawn along the core is assessed for certain parameters (here lithology, clast frequency, size, sorting, roundness, and grain or matrix support) (Suppl. Data 1). The cut-off size used for Site M0077 in Chicxulub and for all aforementioned craters was 5 mm, except for Wetumpka where it was 1 mm. Thus, to enable comparisons, for Wetumpka we included only clasts  $\geq 5$  mm (Suppl. Data 2). The clast size recorded for clasts larger than the core diameter is the apparent maximum size along the vertical core axis. The 1 m-length Vakkejokk cores do not allow the here applied statistical treatment and are excluded from our comparative study. For Chicxulub Site M0077, the line-logging technique was applied for the first time to high-resolution core photos with the use of the image analysis software jMicrovision (version 1.2.7).

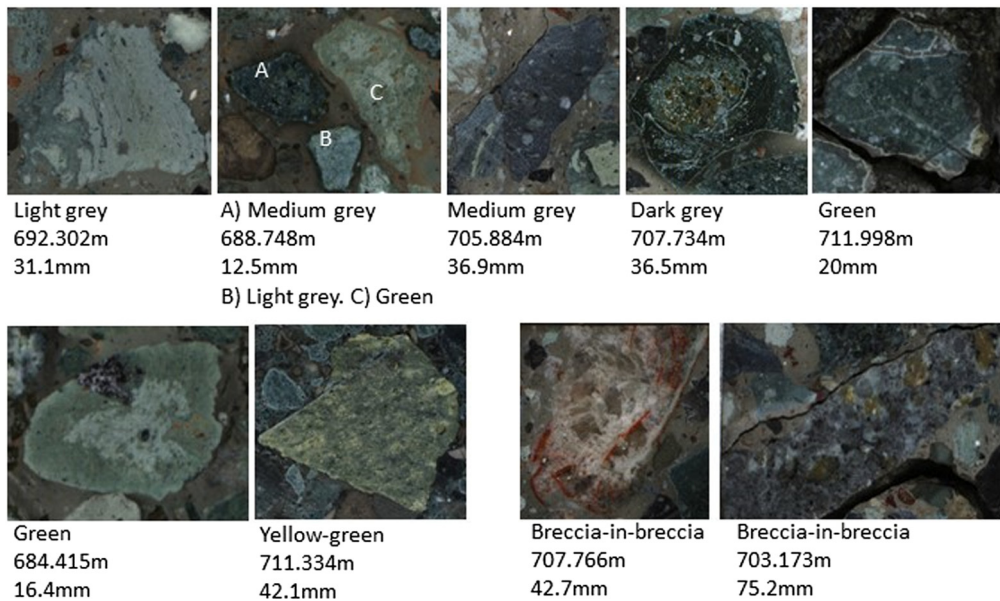
In the suevite (Hole M0077A Units 2A, B), 2376 clasts were analyzed between depths 672.01 mbsf and 715.93 mbsf. Represen-

tative core photos are presented in Fig. 2 and of the clasts in Fig. 3. The 5 mm cut-off has the consequence that the finer-grained the sediment becomes, the more artificially skewed the clast-size populations become when plotted in histograms for each respective meter. This method was first described by Örmo et al. (2007) to determine the level in the core at which the obtained clast size data becomes unreliable, and we have applied it also in this study (Suppl. Data 1). When coupled with an obvious drop in number of clasts per meter, despite a fine-grained, clast-supported appearance (i.e., above 679 mbsf in the M0077A core), we conclude a reduction in reliability of the clast-size data above this level (Fig. 4). After observation of skewed clast-size populations and a reduction in clasts per meter were established, upwards logging was discontinued. At Site M0077, logging was extended downward 3 m into the lithological unit 2C underlying the graded suevite to obtain some reference data points from that unit (cf. Gulick et al., 2017a, 2019) (Fig. 4).

The recovery of drill core at the Site M0077 was as high as 99% (Gulick et al., 2017a). Nevertheless, there were 5 sections with losses  $>32\%$  per meter which we excluded: 689 mbsf (54%), 690 mbsf (46%), 694 mbsf (100%), 695 mbsf (90%), 701 mbsf (58%), and 704 mbsf (74%). Clast frequency data points for the 3 intervals with 17–32% core losses are put in brackets in the plots. Other data for these points are not significantly affected.

Here, lithologies were determined by appearances in core photos in visible light bandwidth with respect to texture, color, visible mineral crystallinity and/or macro-fossils. X-Ray computed tomography (CT) images aided the lithological determinations as these data can be used as proxies for density, composition and display

## 1. Melt particles (altered) and ‘breccia-in-breccia’



## 2. Upper target (varieties of carbonate)

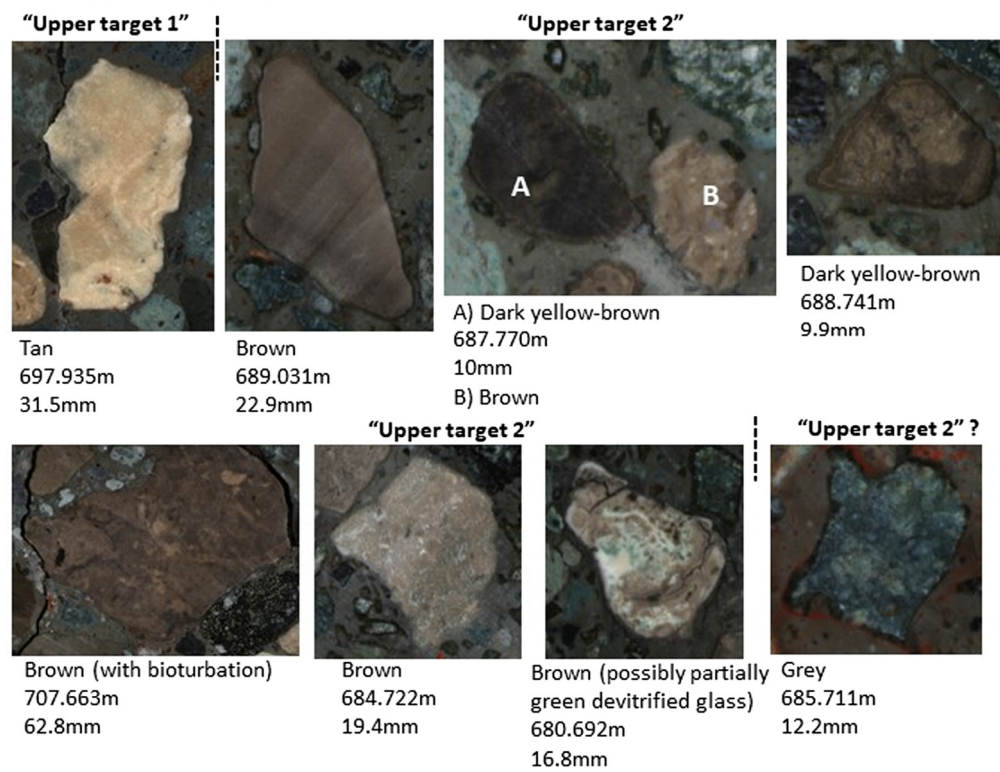
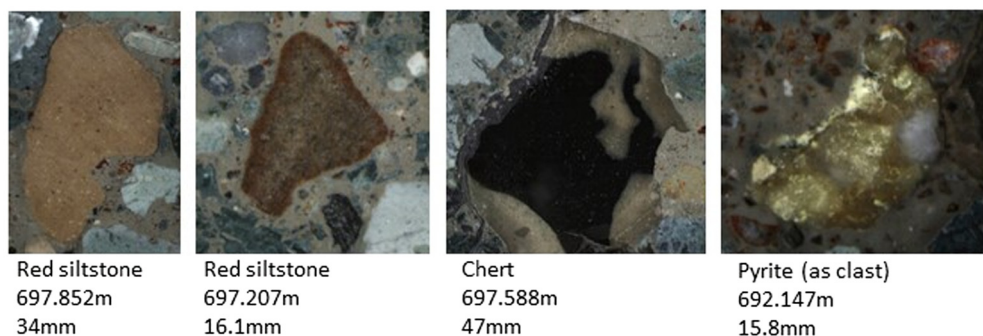
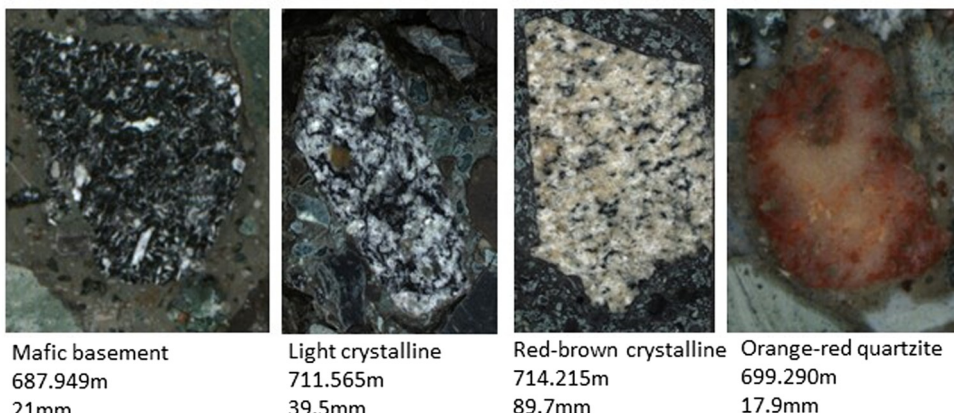
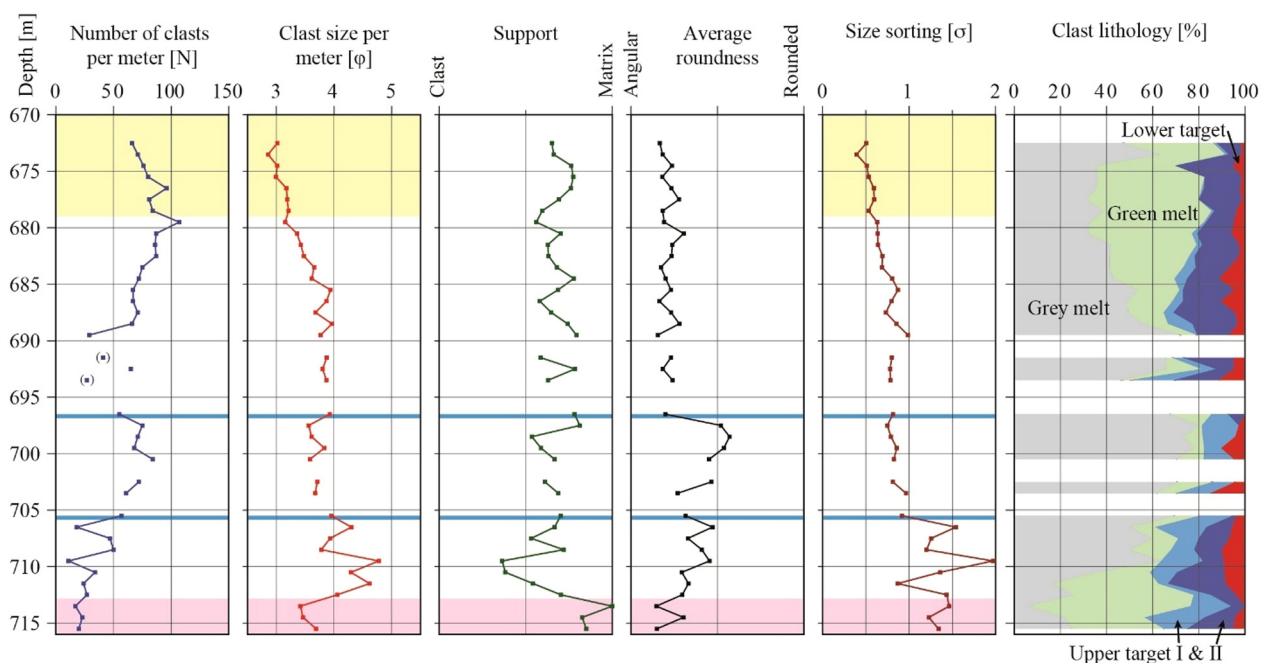


Fig. 3. Clast classification.

internal structure of the cores (Gulick et al., 2017b). Granulometric data were treated as variations per meter, which allowed plots of clast frequency per meter (here called  $N$ ) and size sorting. Clast sizes are given as mean  $-\Phi$  values per meter (here called  $\varphi$ ), and sorting is determined by the standard deviation ( $\sigma$ ) of this value (cf. Ormö et al., 2007). Evaluation of matrix- or clast support of each grain is based on contact with adjacent clasts. Roundness was estimated with a grain shape comparator. Here, a diagram with angular, sub-angular, sub-rounded, and rounded was used (cf., Mazzullo et al., 1988). Clast vs. matrix support was plotted as a ra-

tio per meter and show relative variations, indicating trends, but should not be seen as a source for absolute values for specific parts of the core.

We classified 17 lithologies that subsequently were grouped into 3 categories: “Melt particles and breccia-in-breccia”, “Upper target”, and “Lower target” (Fig. 3). “Upper target” was subdivided into “Upper target I”, “Upper target II” and “Upper target; Other”. Descriptions of the target succession by Kring (2005) were used to categorize the lithic fragments. The term “Melt particles” is adapted from, and the particles classified according to, Wittmann

**"Upper target; Other"****3. Lower target****Fig. 3. (continued)**

**Fig. 4.** Graphs showing variation in granulometry, clast support, and clast lithology in the M0077A core. Yellow fields indicate parts of less reliable data due to effects from the 5-mm cut-off, and pink fields due to the different lithology of unit 2C (See Methods). Note that the 5-mm cut-off only affects clast frequency, clast size, and size sorting. Likewise, the data from unit 2C are less reliable due to some clasts being larger fragments of the underlying clast-rich melt rock, and thus not necessarily a clastic deposit. Horizontal blue lines indicate levels of significant change in the depositional regime; Lower part: Mainly ground-hugging flow and MWI. Middle part: Boundary bed with short-transported rip-up by the resurge. Top part: Settling during decreasing transport energy of the resurge. Lithology log: 'Lower target' represents crystalline basement and quartzite. 'Upper target I' represents tan carbonates that likely come from the upper part of the Yucatán Group, and 'Upper target II' brown carbonates that likely come from the lower part of the same. All data plots except for the lithology distribution have been published by Gulick et al. (2019, Fig. 3) in a comparison with data from machine learning analysis.

et al. (2007) on the melt particles in the Yaxcopoil-1 drill hole located at the outer portion of the terrace zone (Fig. 1). The “melt particles” are not still in the form of “melt” *sensu stricto*, but are “devitrified glass” shards, or sporadically, and mainly in the lower part, altered crystalline “melt rock” fragments (cf. Simpson et al., 2020; Gulick et al., 2017c; Osinski et al., 2020).

Uncertainty estimates (Suppl. Data 2) include 5% human error on clast frequency and a water depth uncertainty based on published paleobathymetry depths reported for each crater. More challenging is the interrelationship of crater diameter, impactor size ( $d$ ) and impact velocity ( $v$ ) where final crater size is proportional to  $d * v^{0.58}$  (Ivanov, 2005). As our final analysis requires an uncertainty estimate on  $d$ , we hold the crater size constant for each crater but vary the impact velocity to generate an uncertainty in final diameter of the impactor. These uncertainties are then combined using a square root of the sum of the squares method (Suppl. Data 2).

### 3. Results

#### 3.1. Clast lithologies and provenance

The lithology categories are shown in Fig. 3. They are: 1) “Melt particles” and “breccia-in-breccia”; 2) “Upper target” that include carbonates, a few other sedimentary rock clasts (i.e., siltstone), and upper target derived material (e.g., chert nodules, pyrite); and 3) “Lower target” that includes clasts of crystalline rock and quartzite. Notwithstanding that the bulk of the melt particles in the graded suevite has been altered to clay (Simpson et al., 2020) as also noted both in Yaxcopoil-1 and distal ejecta in Belize (Wittmann et al., 2007; Pope et al., 2005), we divide the melt particles into two groups based on color in core photos: 1) various shades of green, and 2) various shades of grey (Fig. 3). Simpson et al. (2020) also noted color variations, but in transmitted light, and associated them with distinct precursor melt compositions, one more mafic (“brown-black”, which likely corresponds to our grey clasts) and one more felsic (“green-yellow”). Despite being altered, the fragments often retain vesicular and flow-banded textures typical of devitrified glass shards in the Yaxcopoil-1 core (Wittmann et al., 2007). Grouped with melt fragments mainly between 703 and 708 mbsf are six clasts of ‘breccia-in-breccia’, each clast itself consisting of melt rock fragments in an altered melt matrix (Fig. 3). The relative distribution of the main clast categories (i.e., Grey melt, Green melt, Upper target I, II and Lower target) is shown in Fig. 4 together with granulometric data.

Based on comparisons with field observations in Belize-Guatemala-México, as well as stratigraphic columns (King and Petruny, 2020 and references therein), the upper target carbonates could be further subdivided into two main groups for more hints of their provenance (Fig. 3, Fig. 4). “Upper target I” carbonates are distinctively tan colored in contrast to the brown carbonates of “Upper target II” (Fig. 3). The tan carbonates likely come from the upper Yucatan Group, which is equivalent of the informal Barton Creek formation in Belize (~450 m thick in northern Belize; King and Petruny, 2020) and the Campur Formation of Guatemala, and brown and grey carbonates likely come from the lower Yucatan Group, which is equivalent of the informal Yalbac formation of Belize (~1350 m thick in northern Belize;) and of the Coban Formation of Guatemala (King and Petruny, 2020 and references therein). The grey carbonates were very rare (12 specimens) at 681–692 mbsf and 703–714 mbsf. Their distribution in the core may indicate an affinity to “Upper target II”.

The interval between 697 and 706 mbsf is characterized by a near absence of the otherwise rather common brown carbonate (Upper target II) and green melt particles. Instead, this interval is dominated by grey melt particles and an unchanged amount

of tan carbonate (Upper target I) and lower target rocks (Fig. 4). Above 697 mbsf “Upper target II” dominates the target rock clasts, and green melt particles over grey. Notably, our logging did not encounter any evaporites otherwise very common in the target (Gulick et al., 2019). The contribution to the deposits from crystalline lower target rocks remains relatively equal throughout the logged interval.

#### 3.2. Granulometry and clast support

The number of clasts increase linearly upwards until the effect of the 5-mm cut-off size becomes noticeable as a drop in number of clasts above 679 mbsf (Fig. 4). In reality, the number of clasts increases above that level as the sediment continues to fine upwards (Gulick et al., 2019). Below 706 mbsf, the clast size and sorting, as well as matrix/clast support varies strongly. Between 697 and 706 mbsf the clast frequency and roundness reach distinctive peaks (Figs. Suppl. Mat. S1, S2); the observed peak is due to all lithologies exhibiting greater roundness, although especially the green melt particles and lower target rocks. The high clast frequency is coupled with a slight drop in clast size whereas the matrix content remains unchanged. The sorting improves noticeably and remains in the range 0.5–1.0 throughout the rest of the logged interval, which is defined as moderately to moderately well sorted (Folk, 1974).

At 697 mbsf, there is a slight, but abrupt coarsening and a slight shift to higher matrix content (Fig. 4). Notably, no obvious discontinuity surface could be seen at this level. The clast size shift is followed by a normal grading that then is accentuated at 685 mbsf. Matrix content remains essentially the same. At 697 mbsf there is also a distinct break in the otherwise upwards increase in roundness where it reverts to a level of high angularity that continues to the top of the logged section.

### 4. Discussion

#### 4.1. Mode of transport and deposition

Gulick et al. (2019) included the granulometry data presented here for their graphical reconstruction of the formation, and subsequent modification, of the Chicxulub crater. They describe the resurge entering the impact basin as a forceful flood mainly from the deep-water NE sector and how the crater is filled within hours after the impact. Here, we go into detail on the sedimentological features that form the base for the resurge process reconstruction and compare with similar deposits from other marine-target craters.

Beginning near the base of the logged interval and moving upwards, we see that melt rock in unit 2C below 712.84 mbsf (Fig. 2) often occurs as matrix between lithic clasts, but also as clusters of melt rock clasts with good fitting (i.e., breccia with non-rotated clasts). The drastic change at 710 mbsf from a dominance of green melt particles to grey (Fig. 4), and above 706 mbsf to completely occur as isolated, small devitrified glass shards, may indicate a shift in source from direct incorporation of melt rock fragments from the crater floor (local source), to predominantly longer transported particles possibly originating as ejecta. In addition, below 706 mbsf the deposits show no sign of having been sorted by water whereas there is a clear sorting above that level (Fig. 4). Gulick et al. (2019) suggested that these lower deposits formed by a combination of ground-hugging flows (similar to pyroclastic ignimbrite flows) and resurfacing water meeting with impact melt on the crater floor causing explosive melt-water-interactions (MWI) (Osinski et al., 2020). Phreatomagmatic explosions would loft melt rock fragments and rapidly quenched glass shards into the water column,

which then also is charged with rip-up target rock clasts and proximal ejecta as is envisaged for Sudbury (Grieve et al., 2010) and Chicxulub (Osinski et al., 2020). Below 706 mbsf, there is also a relatively equal co-occurrence of clasts from "Upper target I and II", material that was displaced, but not ejected, during the expansion of the crater. Notably, the rare breccia-in-breccia clasts may represent short transported rip-up material of melt particles of unit 2c.

The above 706 mbsf increase in grey melt rock clasts, and near absence of brown carbonates ('Upper target II') may indicate the majority of the deposit to have been transported from another source area within the crater. The lithology variations in Fig. 4 suggest that the base of the resurge may have had some preferential rip-ups of melt clasts over target rock. This relationship is consistent with the resurge transited across a crater floor that already was largely made up of impactoclastic flows (Gulick et al., 2019), but the MWI process likely contributed where large volumes of intact melt were encountered. Through these processes a boundary layer near the base of the resurge develops when it transits across the crater to crest the peak ring. It leaves a ~9 m thick layer (i.e., 697–706 mbsf) with higher roundness, grading and greatly improved sorting indicating that these sediments were water-borne. Possibly, the observed variations in granulometry and composition of the boundary layer and surrounding deposits are a result of conflicting interaction of two water masses at the peak ring. One would come in from NE (deepest water and gap in the inner rim) (Fig. 1), move across the muted peak ring in that area, across the central melt sheet region undergoing MWI and then crest the peak ring. The other mass would come in from NE but channel around the peak ring in the annular trough and lap up onto the peak ring from the outside inwards and might also have some MWI from melt that made it into the annular trough.

Simpson et al. (2020) observe that between 689 and 706 mbsf there is a distinct increase in porosity and chemical alteration, especially affecting the metastable silicate glass that was the origin of the logged melt particles described here. Fig. 4 shows that this interval coincides with the drop in the fraction of green melt particles. If the color change is due to later alteration then it would contradict the suggestion by Simpson et al. (2020) that the green (felsic) glass is more resistant to alteration than the glass of mafic origin.

Above 697 mbsf, the continued resurge caused a general fining-up sequence with maintained good sorting indicating settling from a suspension flow with waning transport energy (Gulick et al., 2019). At 685 mbsf the normal grading is further accentuated, probably due to fast drop in transport energy when the crater is now becoming filled with water. This continued increase in sorting and reduction in clast size is consistent with MWI only occurring early in the process (Gulick et al., 2019) and not continually throughout crater infilling.

The reason for the higher degree of roundness of clasts of all lithologies in the ~9 m thick boundary layer (706–697 mbsf) could be an effect of shear stresses along the base of the resurge, but our analysis (Fig. Suppl. Mat. S2) indicates it is rather preferential sorting due to clast shape (i.e., the clast drag coefficient) with angular clasts settling slower than equal-sized rounded clasts of the same lithology (cf., White, 1999). This finding means that the processes causing the roundness distribution are general for all lithologies, and not specifically linked to a certain process such as the MWI. The angular melt particles may have formed from physical interactions between impactoclastic flows and melt, from MWI during the earliest stages of resurge, or from melt in proximal ejecta that rapidly quenched and fragmented in contact with the seawater (cf. Dressler et al., 2004). The latter interpretation may be supported by the strong upwards change in color of the melt particles (i.e., from grey to predominantly green) as angular, commonly green,

melt particles weathered to clay in distal carbonate ejecta units exposed in northern Belize (~400 km from crater center) (Pope et al., 2005).

It is notable that the increase in the amount of green melt particles above 697 mbsf occurs together with an increase in the amount of "Upper target II" carbonate clasts. Likewise, in Fig. 3 an "Upper target II" brown carbonate clast is closely associated with what seems to be green devitrified glass. This covariation of green melt particles and "Upper target II" carbonates, together with the slight, but distinct, shift towards coarser clast sizes above 697 mbsf may further support that material above 697 mbsf represents a slightly more energetic pulse of the resurge with more long distance-transported material still in suspension. This second pulse could be linked with the aforementioned possible collision of water masses diverging around the peak ring and reminiscent of the collapse of the central water plume and subsequent anti-resurge indicated in the Lockne cores (Ormö et al., 2007). Site M0077 at the WSW side of the peak ring is also at a location where deep resurge from the NE could meet a shallow resurge from the W and SW and/or get reflected against the inside of the higher relief crater rim (cf. Gulick et al., 2019, Fig. 2).

Reverse stratigraphic ages of clasts were also noted in the Tvären crater (Ormö, 1994) and may indicate clast provenance. Numerical modeling of Lockne (Lindström et al., 2005a) as well as clast component analysis for Lockne, Tvären and CBIS (Ormö et al., 2007, 2009) showed that rip-up from the seafloor and ejecta near the crater rim was a main contributor of sedimentary clasts to the resurge flow. Possibly, uppermost Chicxulub target material was to a higher degree incorporated with seawater in the unstable transient crater rim wall, whereas material from deeper parts of the target was predominantly forming the overturned flap. Thus, material from the "Upper target I" would have been included first in the resurge followed by rip-up of the "Upper target II", which then, together with other ejecta material (e.g., melt particles), would continue to arrive to the investigated drill site on the peak ring during the duration of the resurge. However, the absence of evaporites known to constitute a substantial portion of the upper target sediments (e.g., Rebollo-Vieyra and Urrutia-Fucugauchi, 2006) indicate that, for some reason, these were not included in the resurge transport. Gulick et al. (2019) suggest this absence of evaporite clasts to be either preferential ejection of evaporites through large fragment generation or preferential vaporization.

Of well-characterized marine-target craters with line-logged graded sequences (Table 1) the clast-frequency, size and sorting trends seen in the logged section of the graded suevite of core M0077A show the most similarities to the resurge deposits observed in the relatively deep-water impact craters Lockne (7.5 km wide) and Tvären (2 km wide) (cf. Ormö et al., 2007 and Suppl. Data 2). Importantly, these graded sequences, just like in Hole M0077A, also show direct transitions into post-impact, marine pelagic rocks that display secular variations (Whalen et al., 2020; Lowery et al., 2018; Frisk and Ormö, 2007). A significant difference between the Chicxulub graded suevite and the resurge deposits at Tvären and Lockne is the distribution of high-shock material (e.g., melt particles) wherein at the smaller craters these mainly occur in the finest grained parts of the deposits (i.e., below the 5 mm cut-off) (Theriault and Lindström, 1995; Lindström et al., 1994, 2005b). This difference is likely due to significantly greater energy of the Chicxulub event relative to these much smaller impacts producing relatively more melt to be incorporated into impactoclastic flows, ejected, and/or to contribute to the MWI process (cf. Grieve and Cintala, 1992; Grieve et al., 2010; Osinski et al., 2020).

**Table 1**  
Core data from craters formed at different relative target water depths ( $d/H$ )<sup>\*</sup>.

Crater	$d/H$	Core	$\langle N \rangle$	$\langle -\Phi \rangle$	Description
Lockne	1.2	Lockne-1	133	3.2 (9 mm)	Just inside crater rim. Suspension deposit. Fines are kept relatively longer in suspension in this collision zone between the resurge and the anti-resurge from the collapsing central water plume. This gives a more 'washed' appearance than Lockne-2.
		Lockne-2	85	3.5 (11 mm)	In moat. Muddy matrix. Suspension deposit (hyperconcentrated). Rapid deposition after collapse of central water plume. Target lithologies mainly crystalline and some limestone.
Chicxulub	6.1	M0077A	72	3.6 (12 mm)	On peak ring. Muddy matrix. Suspension deposit (hyper-concentrated). Target lithologies mainly crystalline and sedimentary (mostly carbonates and evaporites).
Tvären	2	Tvären-2	69	3.7 (13 mm)	At center of a simple crater. Muddy matrix. Suspension deposit (hyper-concentrated). Target lithologies similar to Lockne.
Flynn Creek	4.2	67-3	40	3.9 (15 mm)	In moat. Muddy matrix. Suspension deposit (hyperconcentrated towards debris flow).
		77-3	32	4.0 (16 mm)	In moat. Muddy matrix. Suspension deposit (hyperconcentrated towards debris flow).
					Target lithologies mainly dolomites.
CBIS	11	Eyreville A	7	4.3 (19 mm)	In moat. Mainly debris flow.
		Langley	6	4.4 (21 mm)	Inside rim of annular trough. Mainly debris flow.
					Target lithologies crystalline basement covered by poorly consolidated siliciclastic sediments.
Wetumpka	6.7	09-03	2	3.8 (14 mm)	Inside crater (simple). Mudflow deposit. Target similar to CBIS.

\*  $H$  is target water depth and  $d$  is impactor diameter, both from literature. If varied water depth over the target area the figure for the deep-water side is used as the deepest flow had most effect on deposition (Ormö et al., 2010a).  $\langle N \rangle$  is the mean clast frequency per meter, and  $\langle -\Phi \rangle$  the mean clast size for the resurge deposits within given cut-off boundaries (see Methods). For source data for Chicxulub see Suppl. Data 1 and for the other craters Suppl. Data 2 and references therein. The cores are ordered based on the  $\langle N \rangle$  values.

#### 4.2. The character of the resurge flow

At Chicxulub, the upwards transition into marine secular sediments represented by a ~90 m thick, generally fining-up sequence (Gulick et al., 2019), and comparison with complete resurge sequences (from the onset until the secular sedimentation) of other marine-target impact craters such as Lockne, Tvären, CBIS, Wetumpka, and Flynn Creek (cf., Ormö et al., 2007, 2009, 2010b; De Marchi et al., 2019), allows the interpretation that deposition of the here logged section occurred from a single, forceful resurge followed within the same day by seiches, oscillations and returning tsunami reflected off from distant shores (Gulick et al., 2019 and references therein). To allow the transport in a suspension flow capable of generating a single graded sequence of this thickness the amount of available water must also have been large.

Factors that would influence the amount of water in the transported medium are: i) the relative target-water depth (as compared to diameter of impactor), and ii) the type of target. Water depth controls the amount of water available for transport of entrained material. Therefore, it seems logical that a small crater formed in deep water will have resurge deposits that are more strongly influenced by the effects of water than a much larger crater at the same water depth. This notion applies when considering the differences in the quantity of debris from ejecta and from rip-up. Regarding the second factor, an impact into a target with

poorly consolidated sediments likely has a greater influx of eroded debris within its resurge than an impact into a harder, less readily eroded target.

Table 1 distills the available resurge-related data for marine-target impact craters (Suppl. Data 2) including our analysis of Chicxulub presented here (Suppl. Data 1). The parameters include the relation between impactor diameter ( $d$ ) and target water depth ( $H$ ) as a way to relate the water depth to the magnitude of the event, and the average clast frequency per meter (here  $\langle N \rangle$ ) as well as the mean clast size (here  $\langle -\Phi \rangle$ ) for the part of the resurge deposits in the cores that are statistically reliable (See Methods). Critically, we also note the sedimentology, interpreted flow character, and location within the respective craters of the examined drill sites to place these values in context (Fig. 5).

By plotting the relation between mean clast size per meter ( $\varphi$ ) and the number of clasts per meter ( $N$ ) we analyze whether it is the amount of matrix or number of large clasts that influence the clast frequency (Fig. 6a, 6b, Fig. 7). As Lockne-2 spans both resurge deposits (i.e., the Lockne Breccia, cf. Ormö et al., 2007) and avalanche/slump deposits (i.e., the Tramsta Breccia, cf. Sturkell et al., 2013) it is evident that there is a clear distinction between these types of deposits (Fig. 6a). In our comparison with the Lockne-2 resurge deposits we have applied the lower boundary at 215 m (Ormö et al., 2007) (for this and other core boundaries see Suppl. Data 2). However, as Fig. 6a shows some spurious points it was necessary to investigate position in the core (Fig. 6b). By

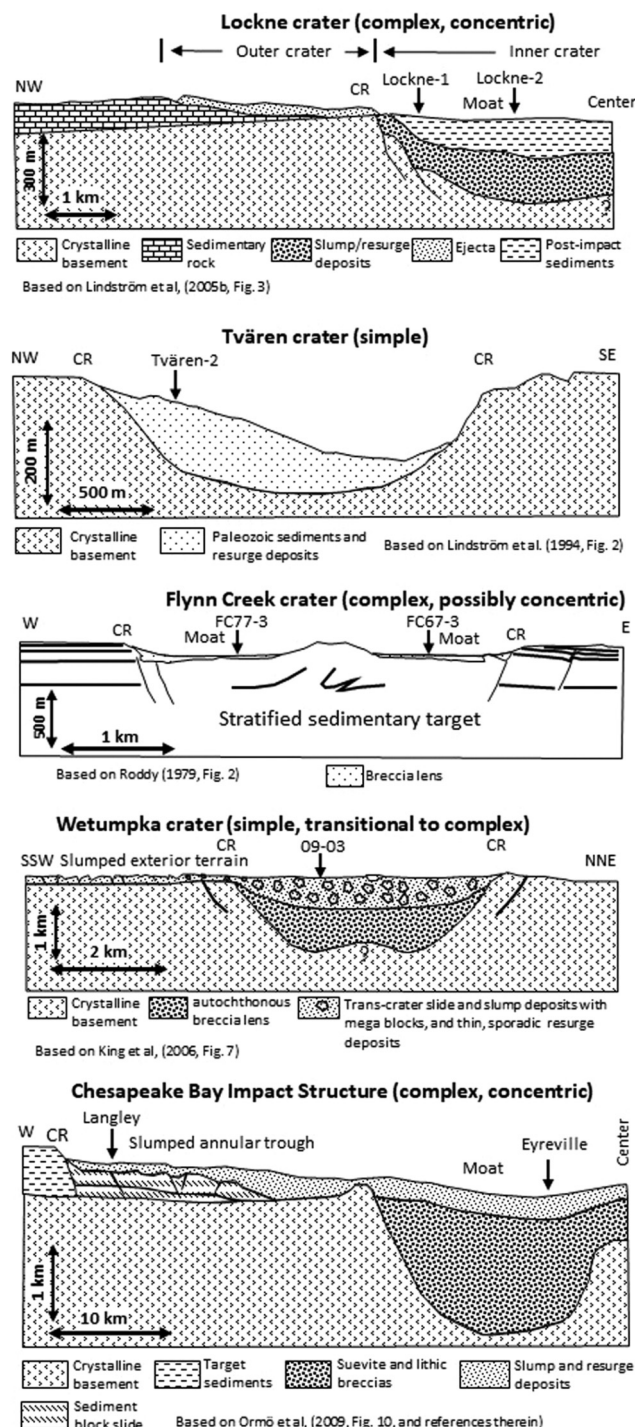


**Fig. 5.** Schematic crater profiles of the included craters illustrating the relative topographic locations of the discussed drill cores. For Chicxulub see Fig. 1. The locations of the apparent crater rims as most commonly given in literature for each crater are indicated by "CR". For Lockne, Ormö et al. (2013) argue the real extent of the crater is best represented by the limit of the outer crater. A concentric crater morphology is a consequence of target layering and includes a nested, deeper crater in the basement surrounded by a shallow, outer crater in the upper layer (often sedimentary rock) (See Ormö et al., 2013 and references therein). It can form either during crater excavation phase (e.g., Lockne), or by extensive slumping of poorly consolidated sediments during crater modification phase (e.g., CBIS). The former is considered in calculations of the projectile diameter whereas the latter generates a larger apparent crater than represented by the projectile size (See Suppl. Data 2). At Wetumpka the upper layer collapse was limited to a narrow sector ("slumped exterior terrain") and has, thus, not been considered part of the apparent crater diameter. For simplicity, the model by Roddy (1979) for Flynn Creek is chosen although recently a more concentric morphology has been suggested (Adrian et al., 2019).

applying a quotient  $N/\varphi$  (here set to 15 as it seems to most obviously separate the spurious readings from the majority) we can evaluate the influence of 1) a larger proportion of clasts smaller than the 5 mm and 2) when a different regime of deposition (e.g., slumping) dominates. For Lockne-2, it is clear that these two effects occur in the boundary zones of the here studied resurge interval (170–215 m, Ormö et al., 2007) (Fig. 6b). For Tvären-1, the selected interval (66–82 m) is not affected (Fig. 6b). Fig. 7 shows a similar plot as Fig. 6a for the cores from the other craters. Thus, we can show that clast frequencies are predominantly controlled by matrix content and only in a very few cases by the occurrence of large blocks. Therefore, we are confident that for the analyzed resurge deposits a high clast frequency indicates a water-rich flow, whereas a low frequency indicates a high matrix content.

In Table 1, the Lockne crater (especially the Lockne-1 core) with its relatively water-rich resurge and consolidated seafloor target rocks is at one end of the scale (with suspension deposits), whereas the CBIS is affected by its larger size relative to the target water depth in combination with a great thickness of poorly consolidated target sediments providing a relatively higher amount of material to the resurge flow. A similar target situation is also known for the, albeit smaller, Wetumpka crater, which similarly to CBIS led to extensive slumping and blending of loose material with a limited amount of available water (King et al., 2006). In the latter two craters, the resurge sediments are in the form of debris and mudflow deposits (Örmö et al., 2009, 2010b). On the other hand, Flynn Creek falls in a transition between the mud/debris flows of CBIS and Wetumpka and the more water-rich flows of Lockne, Tvären and Chicxulub (Fig. 6a, 6b, Fig. 7).

A flow with a sediment load of 20–60%vol is generally described as hyperconcentrated (cf. Vallance, 2000). Despite the high matrix content deposits from such flows often maintain a normal grading (e.g., Ormö et al., 2007). From Figs. 4 and 7, we can assume a maximum sediment load of 20%vol for Chicxulub resurge. Thus, when counting with only a finite amount of the deposits having been added by the later reflected tsunami, the flow over the peak ring would have been approximately  $5 * 90$  m, or 450 m deep. Despite the elevated position, the obtained flow depth and sediment load is similar to that of the Lockne resurge for which numerical simulation showed flow velocities in the order of several tens of meters per second (Shuvalov et al., 2005), basically hurricane velocities but in a dense medium. Notably, this calculation is for the location of Site M0077 on top of the peak ring that was  $\sim 500$  m in relief above the crater floor (Gulick et al., 2019). Possibly, as mentioned above, the Site M0077 is in a collision zone of the resurge with similar effects on deposition as the for Lockne-1 conflicting resurge proper and anti-resurge. This led to material being kept in suspension relatively longer (i.e., a prolonged 'washing') and, thus, a relatively high clast frequency (cf. Ormö et al., 2007, 2010a). Indeed, when plotting the average clast frequencies listed in Table 1 against the ratio between projectile diameter ( $d$ ) and target water depth ( $H$ ) interesting trends emerge that possibly reflect location within the crater and the dynamics of the resurge flow(s) (Fig. 8).

#### 4.3. A new method to calculate target water depth and event magnitude

The advantage of having applied the same method at each of the investigated craters is that it allows direct comparisons of the data (Table 1). Intriguingly, when all ratios of impactor size-to-water depth versus mean clast frequency per meter ( $(N)$ ) for the resurge deposits within the boundaries set by the method are plotted, and their locations within the craters considered, some trends are discernible (Fig. 8). The most obvious seems to be for cores located in relatively low locations within the respective craters such as annular troughs of complex craters or the center of simple

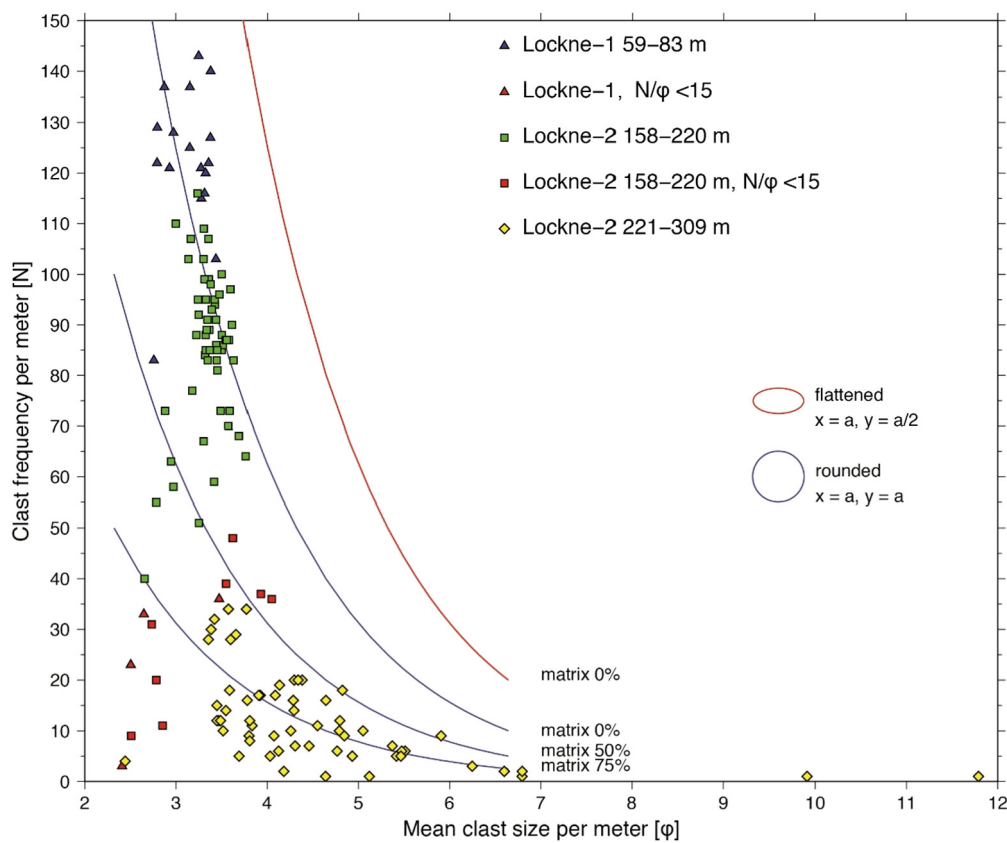


**Fig. 6a.** The effect of matrix and clast size (e.g., eventual occurrences of blocks with dimensions close to or more than 1 m) on the clast frequency for the two Lockne cores (Lockne-1 and Lockne-2). For reference, lines are drawn which represent different matrix amounts depending on the geometry of clasts. In line-logging it is the longest axis that is measured (here “a”). If each meter is composed of clasts positioned next to each other with maximum density then there will be 0% matrix. For spherical clasts this line is marked blue, and is followed by other hypothetical options (50%, 75%) given the increased distance between the logged clasts along the meter line. In a situation with only flattened clasts (for reference here approximated to short axis half of the length axis) laid down as stack of disks (i.e., horizontal length axis) a relatively higher clasts frequency is obtained for the given clasts size. The avalanche/slump deposits in Lockne-2 below the 221 m depth are clearly distinguishable from the resurge deposits above. The reason for the spurious points (red) is analyzed in Fig. 6b. Notably, only the avalanche/slump deposits (yellow) are affected by a couple of meter-sized blocks. The main influence on clast frequency in all deposits is from matrix content. The better size-sorting of the resurge deposits is clearly discernable.

craters (Fig. 5). However, 4 cores; Lockne-1, Chicxulub Site M0077, and the Langley and Eyreville cores from CBIS, fall significantly off the low-location trend line. As there are comparably large uncertainties with the target water depth at the CBIS, (Fig. 8, Suppl. Data 2), we have chosen to exclude CBIS from the trend line calculations. And as two points may make any function, we have chosen to merely indicate what we here call a ‘high location’ trend line (Fig. 8), to account for similarity between the relatively higher position Lockne-1 and Chicxulub M0077 sites.

The CBIS target water depth, as with Wetumpka and Chicxulub, varied over the target area, but the extensive collapse of the CBIS complicates the paleobathymetry assessment of the target area. Horton et al. (2005, p. A16) conclude that the estimated target water depths are in the range of about 0–170 m (mean value 85 m) at the western outer margin, about 40–260 m (mean value 150 m) at the center, and about 80–340 m (mean value 210 m) at the eastern outer margin of the crater. In the plots for craters with varied target-water depths, we use the deeper value for the  $d/H$  ratio as it is expected to be the deep-water flow that dominates the resurge transport (e.g., Ormö et al., 2010a; Gulick et al., 2019). Thus, we apply this assumption also to CBIS. The uncertainty provided by a depth range of 80–340 m (Horton et al., 2005) should be combined with Kenkmann et al. (2009) that use  $H = 500$  m and  $d = 3200$  m in a numerical simulation that allowed the separation of seawater into a separate target layer from the underlying sediments for a better fit between model and cored sediments. Using 500 m, the  $d/H$  would be 6.4 and the CBIS cores

would plot next to Wetumpka on the “low-location” line. However, in Fig. 8 we choose to use the mean of the full plausible depth range 80–500 m, which is 290 m, and the combined uncertainty of 210 m. This gives a  $d/H$  value of 11. Interestingly, this places the CBIS cores right on a hypothetical extension of the “high-location” trend line formed by Lockne-1 and Chicxulub Site M0077 (Fig. 8).

However, the Eyreville core hole (part A drilled to 941 m depth, and B to 1766 m) was drilled in the central, basement crater moat, and the Langley core hole in the “annular trough” just inside the outer rim of the crater (cf. Gohn et al., 2009) (Fig. 5). As neither of these cores are located in any obvious “high” location within the crater maybe the target water depth controlling the resurge deposition was indeed closer to 500 m and, thus, the CBIS cores should belong to the “low position” group as warranted by their positions within the crater. CBIS is the most complicated of the listed craters due to the greatest uncertainties in target water depth, and the extensive expansion by slumping occurring simultaneously with the resurge. It expanded the final crater more than 20 km beyond the size it would have had if directly related to the magnitude of the impact (i.e., 40 km, Collins and Wünnemann, 2005), which consequently led the crater to both reach greater water depths of the shelf as well as creating a structure lacking an elevated rim that could have obstructed the resurge.

Alternatively, the water depth was closer to the 290 m mean, and it is not only the topographic location that affects the deposition. As mentioned earlier, and exemplified by Lockne-1, another discriminating factor affecting the deposits in the analyzed cores

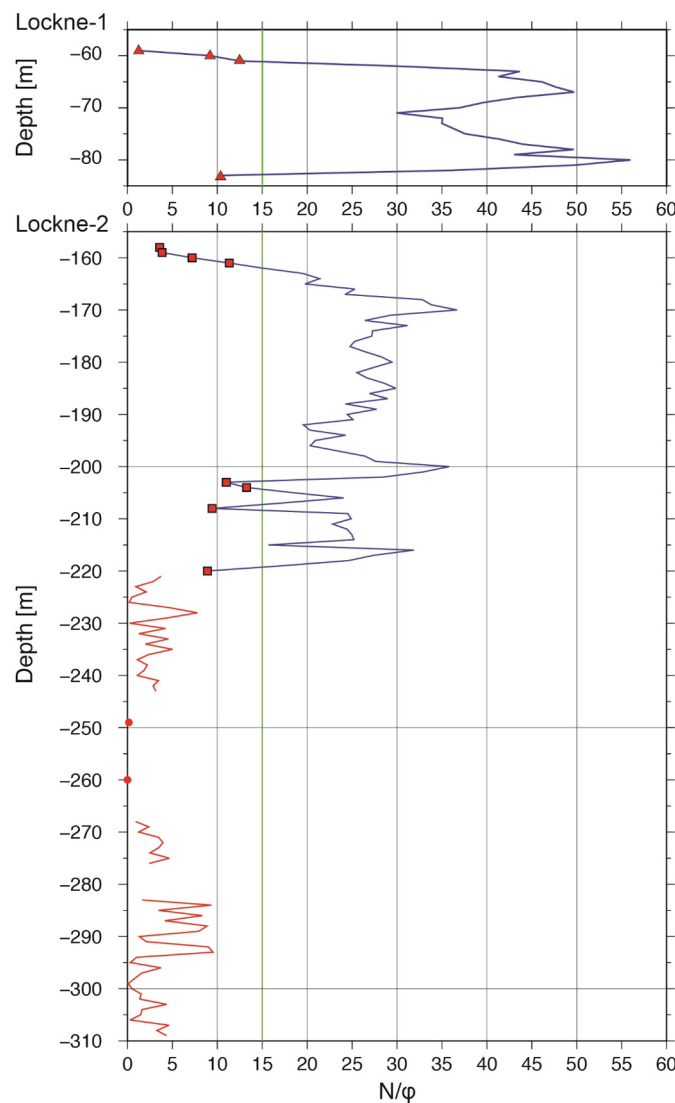


**Fig. 6b.** Analysis of the reason for spurious points (red) in Fig. 6a. We have chosen to make the separation at a value  $N/\varphi = 15$  as points below that value (green vertical line) clearly deviate from the general trend of the resurge deposits (blue graph). Only 3 points in the lower part of the interval used in our study (i.e., 170–215 m) can still be considered to be transitional between slumping and resurge (i.e., 203 m, 204 m, and 208 m). The avalanche/slump deposits of the Tramsta Breccia in Lockne-2 are shown with red graph. In these deposits there are also two large blocks spanning more than a meter each indicated with clear red dots.

is the flow dynamics at the respective location. The collision between the ongoing resurge and the outgoing anti-resurge provided a prolonged influx of energy compared to the Lockne-2 that was more swiftly passed by the effects from the collapsing central water plume. Likewise, all the other cores on the “low-location” trend represent depositional environments where material was more simply settled in a low without the ‘washing-effect’ caused by colliding flows. As noted, Chicxulub Site M0077 on the peak ring would likely have been in a collision zone as well (cf. Gulick et al., 2019, Fig. 2). For CBIS it has been suggested that there was a deeper resurge from the oceanic side and a shallower resurge from the shoreward side, developing a complex set of water plumes and resurge/anti-resurge interactions, likely also coupled with a pulse from the arrival of a tsunami reflected off the coast (Ormö et al., 2009).

Fig. 8 shows a seemingly linear relation between  $\langle N \rangle$  and  $d/H$ . In a preliminary analysis seeking a potential physical explanation, Herreros and Ormö (2020) show that the physical laws governing

particle sedimentation in liquid medium can very closely reproduce the here observed low-location trend. Notably, the relation is only near-linear for the physically feasible span of  $\langle N \rangle$  and  $d/H$  expected to appear in nature. A study of the potential ‘high-location’ (or ‘collision-zone’) relationship has proved more difficult and is pending.

A potential utility of this work is that the equation for the seemingly linear trend of the ‘low-location’ cores (Fig. 8) allow any of the variables: location, clast frequency, projectile diameter, and target-water depth, to be estimated if the three others are known (Eq. (1)).

Low (less turbulent) position at the crater:

$$\langle N \rangle = -15(d/H) + 100 \quad (1)$$

We anticipate that calculations could be done for any crater with available resurge deposits but debated crater sizes or target water depths. Analyses from additional high locations, or potentially sites dominated by convergent flows, could help refine a trend-line equation for these locations as well, which could be tested for a similar utility.

## 5. Conclusions

After the collapse of the transient cavity formed by the Chicxulub impact, a several hundred meters deep ocean resurge flow passed over the melt- and debris-covered crater floor, cresting the ~500 m high peak ring at Site M0077. The hyperconcentrated, mud-charged water carrying material from the whole of the target sequence (except for evaporites) likely caused phreatomagmatic explosions through interaction with impact melt. Ejecta, rip-ups of seafloor sediments, and angular clasts settled last.

When comparing clast frequency data of the Chicxulub resurge deposits with similarly retrieved data from other marine-target craters some relations appear. There is a seemingly linear relationship between the clast frequency and the ratio of impactor diameter and water depth. However, the relationship appears dependent on being either within a deeper location in the crater or possibly requires data from zones of lower energy. This relationship allows for estimation of location, clast frequency, projectile diameter, or target water depth when three of the four factors are independently known.

## CRediT authorship contribution statement

**J. Ormö:** Conceptualization, Methodology, Validation, Formal analysis, Investigation, Data Curation, Writing – Original Draft, Writing – Review & Editing, Visualization, Project administration, Funding acquisition.

**S.P.S. Gulick:** Conceptualization (Co-lead for Expedition 364 and integration with goals & results), Writing – Review & Editing, Visualization, Methodology (statistics).

**M.T. Whalen:** Writing – Review & Editing.

**D.T. King Jr.:** Resources, Writing – Review & Editing.

**E. Sturkell:** Formal analysis, Data Curation, Writing – Review & Editing, Visualization.

**J. Morgan:** Writing – Review & Editing.

## Declaration of competing interest

The authors have no competing interests to declare.

## Acknowledgements

**Funding:** The work by J. Ormö was partially supported by grants ESP2014-59789-P, ESP2015-65712-C5-1-R, and ESP2017-87676-C5-1-R from the Spanish Ministry of Economy and Competitiveness

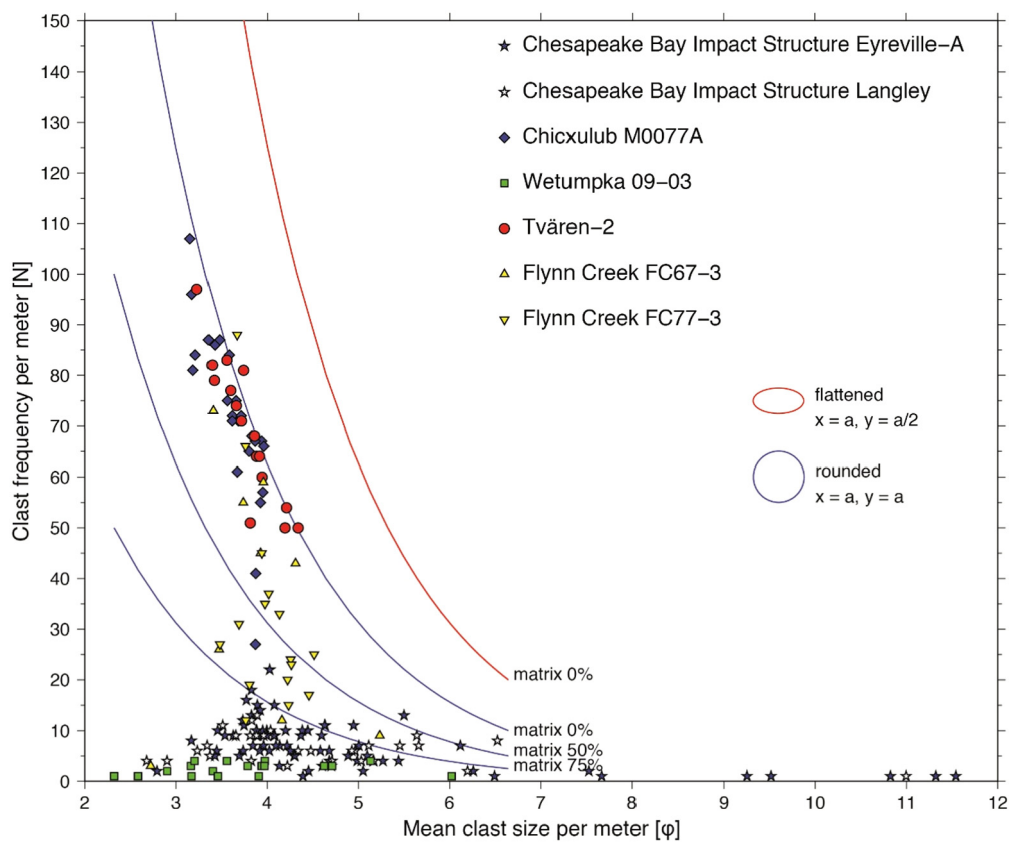


**Fig. 7.** The effect of matrix and clast size (e.g., eventual occurrences of blocks with dimensions close to or more than 1 m) on the clast frequency for the Chicxulub and the other discussed cores (For Lockne cores and explanation to the graphs see Fig. 6a). Notably, only the CBIS cores (blue stars) are affected by a handful of meter-sized blocks. The main influence on clast frequency is from matrix content. Notable is also how a higher water-content of the flow not only influences the clast frequency but also the size sorting.

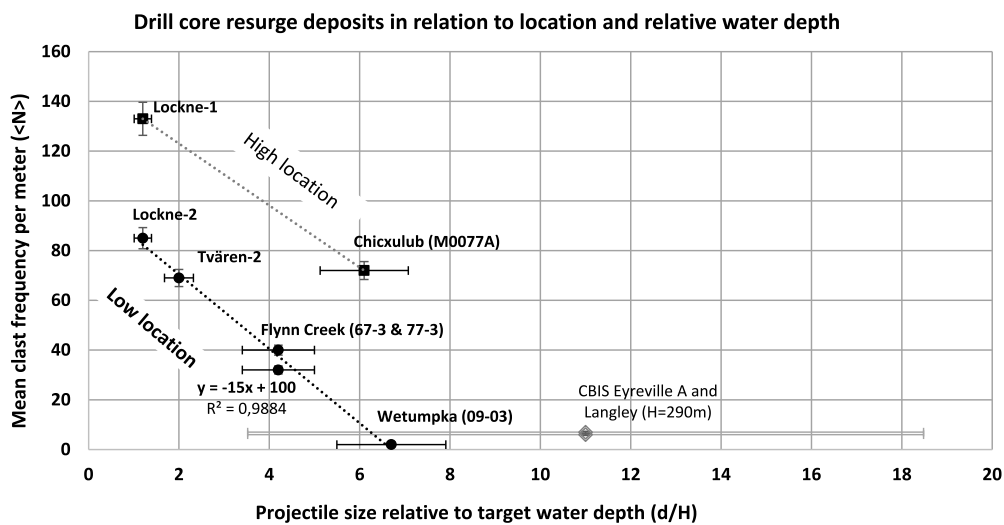


**Fig. 8.** Relation between resurge clast frequency and event magnitude with respect to target water depth and position at the crater for line-logged drill cores from marine-target craters. The relation is suggested to be near-linear for the physically feasible span of  $\langle N \rangle$  and  $d/H$  expected to appear in nature. The cores are plotted with uncertainties presented in Suppl. Data 2. The great uncertainty in the target water depth for the CBIS leads us to exclude the CBIS cores (grey color) from the trend line calculation.

and Fondo Europeo de Desarrollo Regional, the Spanish State Research Agency (AEI) Project No. MDM-2017-0737 Unidad de Excelencia "María de Maeztu"- Centro de Astrobiología (INTA-CSIC), and the Spanish Research Council (CSIC) support for international cooperation: I-LINK project LINKA20203. Morgan was supported by NERC-NE/P005217/1. Whalen was supported by NSF-OCE 14-50528 and 1737199. Gulick was supported by NSF-OCE-1737351. This is University of Texas Institute for Geophysics Contribution #3778

and Center for Planetary Systems Habitability Contribution #0028. The authors are grateful for the valuable comments by Gordon Osinski and an anonymous reviewer.

#### Appendix A. Supplementary material

Supplementary material related to this article can be found online at <https://doi.org/10.1016/j.epsl.2021.116915>.

## References

Adrian, D.R., King Jr., D.T., Ormö, J., 2019. Resurge gullies and 'inverted sombrero' morphology, Flynn Creek impact structure, Tennessee. *Meteorit. Planet. Sci.* 54 (11), 2758–2768. <https://doi.org/10.1111/maps.13387>.

Artemieva, N., Morgan, J., Expedition 364 Science Party, 2017. Quantifying the release of climate-related gases by large meteorite impacts with a case study of Chicxulub. *Geophys. Res. Lett.* 44, 10–180.

Collins, G.S., Wünnemann, K., 2005. How big was the Chesapeake Bay impact? Insight from numerical modeling. *Geology* 33 (12), 925–928. <https://doi.org/10.1130/G21854.1>.

Collins, G.S., Patel, N., Davison, T.M., Rae, A.S.P., Morgan, J.V., Gulick, S.P.S., IODP-ICDP Expedition 364 Science Party, 2020. A steeply-inclined trajectory for the Chicxulub impact. *Nat. Commun.* 11, 1480. <https://doi.org/10.1038/s41467-020-15269-x>.

De Marchi, L., Ormö, J., King Jr., D.T., Adrian, D.R., Hagerty, J.J., Gaither, T.A., 2019. Sedimentological analysis of two drill cores through the crater moat-filling breccia, Flynn Creek impact structure, Tennessee. *Meteorit. Planet. Sci.* 54 (11), 2864–2878. <https://doi.org/10.1111/maps.13393>.

Dressler, B.O., Sharpton, V.L., Schwandt, C.S., Ames, D., 2004. Impactites of the Yaxcopoil-1 drilling site, Chicxulub impact structure: petrography, geochemistry, and depositional environment. *Meteorit. Planet. Sci.* 39, 857–878.

Folk, R.L., 1974. The petrology of sedimentary rocks. Austin, Texas: Hemphill's. 183 p.

Frisk, Å., Ormö, J., 2007. Facies distribution of post-impact sediments in the Ordovician Lockne and Tvären impact craters: indications for unique impact-generated environments. *Meteorit. Planet. Sci.* 42 (11), 1971–1984.

Gault, D.E., Sonett, C.P., 1982. Laboratory simulation of pelagic asteroid impact: atmospheric injection, benthic topography, and the surface wave radiation field. In: Silver, L.T., Schultz, P.H. (Eds.), *Geological Implications of Impacts of Large Asteroids and Comets on the Earth*. In: Spec. Pap., Geol. Soc. Am., vol. 190, pp. 69–102.

Gohn, G.S., Powars, D.S., Dypvik, H., Edwards, L.E., 2009. Rock avalanche and ocean-resurge deposits in the late Eocene Chesapeake Bay impact structure: evidence from the ICDP-USGS Eyreville cores, Virginia, USA. In: Gohn, G.S., Koerber, C., Miller, K.G., Reimold, W.U. (Eds.), *The ICDP-USGS Deep Drilling Project in the Chesapeake Bay Impact Structure: Results from the Eyreville Core Holes*. In: Spec. Pap., Geol. Soc. Am., vol. 458, pp. 587–615.

Goto, K., Tada, R., Tajika, E., Bralower, T.J., Hasegawa, T., Matsui, T., 2004. Evidence for ocean water invasion into the Chicxulub crater at the Cretaceous/Tertiary boundary. *Meteorit. Planet. Sci.* 39 (7), 1233–1247.

Grieve, R.A.F., Cintala, M.J., 1992. An analysis of differential impact melt-crater scaling and implications for the terrestrial impact record. *Meteoritics* 27, 526–538.

Grieve, R.A.F., Ames, D.E., Morgan, J.V., Artemieva, N., 2010. The evolution of the Onaping Formation at the Sudbury impact structure. *Meteorit. Planet. Sci.* 45, 759–782.

Gulick, S.P.S., Barton, P.J., Christeson, G.L., Morgan, J.V., McDonald, M., Mendoza-Cervantes, K., Pearson, Z.F., Surendra, A., Urrutia-Fucugauchi, J., Vermeesch, P.M., Warner, M.R., 2008. Importance of pre-impact crustal structure for the asymmetry of the Chicxulub impact crater. *Nat. Geosci.* 1, 131–135. <https://doi.org/10.1038/ngeo103>.

Gulick, S.P.S., Christeson, G.L., Barton, P.J., Grieve, R.A.F., Morgan, J.V., Urrutia-Fucugauchi, J., 2013. Geophysical characterization of the Chicxulub impact crater. *Rev. Geophys.* 51, 31–52. <https://doi.org/10.1002/rog.20007>.

Gulick, S., Morgan, J., Mellett, C.L., Green, S.L., Bralower, T., Chenot, E., Christeson, G., Claeys, P., Cockell, C., Coolen, M., Ferrière, L., Gebhardt, C., Goto, K., Jones, H., Kring, D., Lofi, J., Lowery, C., Ocampo-Torres, R., Perez-Cruz, L., Pickersgill, A.E., Poelchau, M., Rae, A., Rasmussen, C., Rebollo-Vieyra, M., Riller, U., Sato, H., Smit, J., Tikoo, S., Tomioka, N., Urrutia-Fucugauchi, J., Whalen, M., Wittmann, A., Yamaguchi, K., Xiao, L., Zylberman, W., 2017a. Expedition 364 summary. In: Morgan, J., Gulick, S., Mellett, C.L., Green, S.L., The Expedition 364 Scientists (Eds.), *Chicxulub: Drilling the K-Pg Impact Crater*. In: *Proceedings of the International Ocean Discovery Program*, vol. 364.

Gulick, S., Morgan, J., Mellett, C.L., Green, S.L., Bralower, T., Chenot, E., Christeson, G., Claeys, P., Cockell, C., Coolen, M., Ferrière, L., Gebhardt, C., Goto, K., Jones, H., Kring, D., Lofi, J., Lowery, C., Ocampo-Torres, R., Perez-Cruz, L., Pickersgill, A.E., Poelchau, M., Rae, A., Rasmussen, C., Rebollo-Vieyra, M., Riller, U., Sato, H., Smit, J., Tikoo, S., Tomioka, N., Urrutia-Fucugauchi, J., Whalen, M., Wittmann, A., Yamaguchi, K., Xiao, L., Zylberman, W., The Expedition 364 ESO Team, 2017b. Expedition 364 methods. In: Morgan, J., Gulick, S., Mellett, C.L., Green, S.L., The Expedition 364 Scientists (Eds.), *Chicxulub: Drilling the K-Pg Impact Crater*. In: *Proceedings of the International Ocean Discovery Program*, vol. 364.

Gulick, S., Morgan, J., Mellett, C., Green, S.L., Bralower, T., Chenot, E., Christeson, G., Claeys, P., Cockell, C., Coolen, M., Ferrière, L., Gebhardt, C., Goto, K., Jones, H., Kring, D., Lofi, J., Lowery, C., Ocampo-Torres, R., Perez-Cruz, L., Pickersgill, A.E., Poelchau, M., Rae, A., Rasmussen, C., Rebollo-Vieyra, M., Riller, U., Sato, H., Smit, J., Tikoo, S., Tomioka, N., Urrutia-Fucugauchi, J., Whalen, M., Wittmann, A., Yamaguchi, K., Xiao, L., Zylberman, W., 2017c. Site M0077: upper peak ring. In: Morgan, J., Gulick, S., Mellett, C.L., Green, S.L., The Expedition 364 Scientists (Eds.), *Chicxulub: Drilling the K-Pg Impact Crater*. In: *Proceedings of the International Ocean Discovery Program*, vol. 364.

Gulick, S.P.S., Bralower, T.J., Ormö, J., Hall, B., Grice, K., Schaefer, B., Lyons, S., Freeman, K.H., Morgan, J.V., Artemieva, N., Kaskes, P., de Graaff, S.J., Whalen, M.T., Collins, G.S., Tikoo, S.M., Verhagen, C., Christeson, G.L., Claeys, P., Coolen, M.J.L., Goderis, S., Goto, K., Grieve, R.A.F., McCall, N., Osinski, G.R., Rae, A.S.P., Riller, U., Smit, J., Vajda, V., Wittmann, A., The Expedition 364 Scientists, 2019. The first day of the Cenozoic. *Proc. Natl. Acad. Sci. USA* 116 (39), 19342–19351.

Herreros, I., Ormö, J., 2020. A method to assess event magnitude and target water depth for marine-target impacts. Part 2: the physics behind the observations. In: *EuropaNet Science Congress*, online, 21 September–9 Oct. 2020, #EPSC2020-931.

Horton Jr., J.W., Powars, D.S., Gohn, G.S., 2005. Studies of the Chesapeake Bay impact structure—introduction and discussion, chap. A. In: Horton Jr., J.W., Powars, D.S., Gohn, G.S. (Eds.), *Studies of the Chesapeake Bay Impact Structure—the USGS-NASA Langley Corehole, Hampton, Virginia, Related Coreholes and Geophysical Surveys*. In: *U.S. Geol. Surv. Prof. Pap.*, vol. 1688, pp. A1–A24.

Ivanov, B.A., 2005. Numerical modeling of the largest terrestrial meteorite craters. *Sol. Syst. Res.* 39, 381–409. <https://doi.org/10.1007/s11208-005-0051-0>.

Kenkmann, T., Collins, G.S., Wittmann, A., Wünnemann, K., Reimold, W.U., Melosh, H.J., 2009. A model for the formation of the Chesapeake Bay impact crater as revealed by drilling and numerical simulation. In: Gohn, G.S., Koerber, C., Miller, K.G., Reimold, W.U. (Eds.), *The ICDP-USGS Deep Drilling Project in the Chesapeake Bay Impact Structure: Results from the Eyreville Core Holes*. In: *Geol. S. Am. S.*, vol. 458, pp. 571–585.

King Jr., D.T., Ormö, J., Petruny, L.W., Neathery, T.L., 2006. Role of water in the formation of the Late Cretaceous Wetumpka impact structure, Inner Gulf Coastal Plain of Alabama, USA. *Meteorit. Planet. Sci.* 41 (10), 1625–1631.

King Jr., D.T., Petruny, L.W., 2020. Chicxulub target stratigraphy and ejecta: insights from northern Belize. In: *GeoGulf Transactions*, vol. 70, pp. 143–151.

Kring, D.A., 2005. Hypervelocity collisions into continental crust composed of sediments and an underlying crystalline basement: comparing the Ries (~24 km) and Chicxulub (~180 km) impact craters. *Geochemistry* 65, 1–46.

Lindström, M., Flodén, T., Grahn, Y., Kathol, B., 1994. Post-impact deposits in Tvären, a marine Middle Ordovician crater south of Stockholm, Sweden. *Geol. Mag.* 131, 91–103.

Lindström, M., Shuvalov, V., Ivanov, B., 2005a. Lockne crater as a result of marine-target oblique impact. *Planet. Space Sci.* 53 (8), 803–815. <https://doi.org/10.1016/j.pss.2005.02.005>.

Lindström, M., Ormö, J., Sturkell, E.V., Dalwigk, I., 2005b. The Lockne crater—revision and reassessment of structure and impact stratigraphy. In: Koeberl, C., Henkel, H. (Eds.), *Impact Tectonics*. In: *Impact Studies*. Springer-Verlag, Berlin, pp. 357–388.

Lowery, C.M., Bralower, T.J., Owens, J.D., Rodríguez-Tovar, F.J., Jones, H., Smit, J., Whalen, M.T., Claeys, P., Farley, K., Gulick, S.P.S., Morgan, J.V., Green, S., Chenot, E., Christeson, G.L., Cockell, C.S., Coolen, M.J.L., Ferrière, L., Gebhardt, C., Goto, K., Kring, D.A., Lofi, J., Ocampo-Torres, R., Perez-Cruz, L., Pickersgill, A.E., Poelchau, M.H., Rae, A.S.P., Rasmussen, C., Rebollo-Vieyra, M., Riller, U., Sato, H., Tikoo, S.M., Tomioka, N., Urrutia-Fucugauchi, J., Vellekoop, J., Wittmann, A., Xiao, L., Yamaguchi, K.E., Zylberman, W., 2018. Rapid recovery of life at ground zero of the End Cretaceous mass extinction. *Nature* 558, 288–291. <https://doi.org/10.1038/s41586-018-0163-6>.

Mazzullo, J., Graham, A.G., Braunestein, C., 1988. *Handbook for Shipboard Sedimentologists. Ocean Drilling Program*, College Station, TX, 70 pp.

Morgan, J.V., Gulick, S.P.S., Bralower, T., Chenot, E., Christeson, G., Claeys, P., Cockell, C., Collins, G.S., Coolen, M.J.L., Ferrière, L., Gebhardt, C., Goto, K., Jones, H., Kring, D.A., Le Ber, E., Lofi, J., Long, X., Lowery, C., Mellet, C., Ocampo-Torres, R., Osinski, G.R., Perez-Cruz, L., Pickersgill, A., Poelchau, M., Rae, A., Rasmussen, C., Rebollo-Vieyra, M., Riller, U., Sato, H., Schmitt, D.R., Smit, J., Tikoo, S., Tomioka, N., Urrutia-Fucugauchi, J., Whalen, M., Wittmann, A., Yamaguchi, K.E., Zylberman, W., 2016. The formation of peak rings in large impact craters. *Science* 354 (6314), 878–882. <https://doi.org/10.1126/science.aaa6561>.

Ormö, J., 1994. The pre-impact Ordovician stratigraphy of the Tvären Bay impact structure, SE Sweden. *GFF* 116 (3), 139–144.

Ormö, J., Miyamoto, H., 2002. Computer modelling of the water resurge at a marine impact: the Lockne crater, Sweden. *Deep-Sea Res. II* 49 (6), 983–994.

Ormö, J., Sturkell, E., Lindström, M., 2007. Sedimentological analysis of resurge deposits at the Lockne and Tvären craters—clues to flow dynamics. *Meteorit. Planet. Sci.* 42 (11), 1929–1944.

Ormö, J., Sturkell, E., Horton Jr., J.W., Powars, D.S., Edwards, L.E., 2009. Comparison of clast frequency and size in the resurge deposits at the Chesapeake Bay impact structure (Eyreville-A and Langley cores): clues to the resurge process. In: Gohn, G.S., Koerber, C., Miller, K.G., Reimold, W.U. (Eds.), *The ICDP-USGS Deep Drilling Project in the Chesapeake Bay Impact Structure: Results from the Eyreville Core Holes*. In: *Geol. S. Am. S.*, vol. 458, pp. 617–632.

Ormö, J., Lepinette, A., Sturkell, E., Lindström, M., Housen, K.R., Holsapple, K.A., 2010a. The water resurge at marine-target impact craters analyzed with a combination of low-velocity impact experiments and numerical simulations. In: Gibson, R.L., Reimold, W.U. (Eds.), *Large Meteorite Impacts and Planetary Evolution IV*. In: *Geol. S. Am. S.*, vol. 465, pp. 81–101.

Ormö, J., King Jr., D.T., Harris, R.S., Petruny, L.W., Markin, J.K., 2010b. Sediment laden flow of Moorville Chalk within the interior of Wetumpka marine-target impact

structure, Alabama: evidence for a shallow water resurge. In: 41st Lunar and Planetary Science Conference [#1430].

Ormö, J., Rossi, A.P., Housen, K.R., 2013. A new method to determine the direction of impact: asymmetry of concentric impact craters as observed in the field (Lockne), on Mars, in experiments, and simulations. *Meteorit. Planet. Sci.* 48 (3), 403–419. <https://doi.org/10.1111/maps.12065>.

Ormö, J., Minde, P., Nielsen, A.T., Alwmark, C., 2019. Resurge deposits associated with the shallow marine early Cambrian Vakkejokk impact, north Sweden. *Meteorit. Planet. Sci.* 54 (6), 1246–1261.

Osinski, G.R., Grieve, R.A.F., Hill, P.J.A., Simpson, S.L., Cockell, C., Christeson, G.L., Ebert, M., Gulick, S., Melosh, H.J., Riller, U., Tikoo, S.M., Wittmann, A., 2020. Explosive interaction of impact melt and seawater following the Chicxulub impact event. *Geology* 48, 108–112. <https://doi.org/10.1130/G46783.1>.

Pope, K.O., Ocampo, A.C., Fisher, A.G., Vega, F.J., Ames, D.E., King Jr., D.T., Fouke, B.W., Wachtman, R.J., Kletetschka, G., 2005. Chicxulub impact ejecta deposits in southern Quintana Roo, México, and central Belize. In: Kenkmann, T., Hörz, F., Deutsch, A. (Eds.), Large Meteorite Impacts III. In: *Geol. S. Am. S.*, vol. 384, pp. 171–190.

Rebolledo-Vieyra, M., Urrutia-Fucugauchi, J., 2006. Magnetostratigraphy of the Cretaceous/tertiary boundary and early Paleocene sedimentary sequence from the Chicxulub impact crater. *Earth Planets Space* 58, 1309–1314.

Roddy, D.J., 1979. Structural deformation at the Flynn Creek impact crater, Tennessee: a preliminary report on deep drilling. In: Proceedings, 10th Lunar and Planetary Science Conference, vol. 10, pp. 2519–2534.

Sanford, J.C., Snedden, J.W., Gulick, S.P., 2016. The Cretaceous-Paleogene boundary deposit in the Gulf of Mexico: Large-scale oceanic basin response to the Chicxulub impact. *J. Geophys. Res., Solid Earth* 121, 1240–1261.

Shuvalov, V., Ormö, J., Lindström, M., 2005. Hydrocode simulation of the Lockne marine target impact event. In: Koeberl, C., Henkel, H. (Eds.), *Impact Tectonics*. In: *Impact Studies*. Springer-Verlag, Berlin, pp. 405–422.

Simpson, S.L., Osinski, G.R., Longstaffe, F.J., Schmieder, M., Kring, D.A., 2020. Hydrothermal alteration associated with the Chicxulub impact crater upper peak-ring breccias. *Earth Planet. Sci. Lett.* 547, 116425. <https://doi.org/10.1016/j.epsl.2020.116425>.

Sturkell, E., Ormö, J., Lepinette, A., 2013. Early modification stage (pre-resurge) sediment mobilization in the Lockne concentric, marine-target crater, Sweden. *Meteorit. Planet. Sci.* 48 (3), 321–338. <https://doi.org/10.1111/maps.12058>.

Theriault, A.M., Lindström, M., 1995. Planar deformation features in quartz grains from the resurge deposit of the Lockne structure, Sweden. *Meteorit. Planet. Sci.* 30, 700–703.

Vallance, J.W., 2000. Lahars. In: Sigurdsson, H., et al. (Eds.), *Encyclopedia of Volcanoes*. Academic Press, San Diego, pp. 601–616.

Whalen, M.T., Gulick, S.P.S., Lowery, C.M., Bralower, T.J., Morgan, J.V., Grice, K., Schaefer, B., Smit, J., Ormö, J., Wittmann, A., Kring, D.A., Lyons, S., Goderis, S., The IODP-ICDP Expedition 364 Scientists, 2020. Winding down the Chicxulub impact: the transition between impact and normal marine sedimentation near ground zero. *Mar. Geol.* 430. <https://doi.org/10.1016/j.margeo.2020.106368>.

White, F.M., 1999. *Fluid Mechanics*, 4th edition. WCB McGraw-Hill, Boston. 10:0070697167. 800 pp.

Wittmann, A., Kenkmann, T., Hecht, L., Stöffler, D., 2007. Reconstruction of the Chicxulub ejecta plume from its deposits in drill core Yaxcopoil-1. *Geol. Soc. Am. Bull.* 119, 1151–1167.

Wünnemann, K., Weiss, R., Hofmann, K., 2007. Characteristics of oceanic impact-induced large waves—re-evaluation of the tsunami hazard. *Meteorit. Planet. Sci.* 42 (11), 1893–1903.